Journal of Structural Geology 30 (2008) 1177–1191

Contents lists available at ScienceDirect

Journal of Structural Geology

journal homepage: www.elsevier.com/locate/jsg

Mechanical models of fracture reactivation and slip on bedding surfaces during folding of the asymmetric anticline at Sheep Mountain, Wyoming

Pablo F. Sanz [a,*], David D. Pollard [b], Patricia F. Allwardt [c], Ronaldo I. Borja [a]

[a] Department of Civil and Environmental Engineering, Stanford University, Stanford, CA 94305, USA
[b] Department of Geological and Environmental Sciences, Stanford University, Stanford, CA 94305, USA
[c] ConocoPhillips Subsurface Technology, 600 N. Dairy Ashford, PR2010, Houston, TX 77079, USA

ARTICLE INFO

Article history:
Received 17 September 2007
Received in revised form 3 June 2008
Accepted 5 June 2008
Available online 13 June 2008

Keywords:
Fold
Fracture reactivation
Bed parallel slip
FEM modeling
Frictional contact
Sheep Mountain, Wyoming

ABSTRACT

We use finite element methods to investigate the reactivation of fractures (opening and shearing) and the development of bedding-surface slip during the deformation of the asymmetric anticline at Sheep Mountain, Wyoming. A series of numerical simulations were run to show the effect of mechanical stratigraphy, layer thickness, slip on bedding surfaces, and tectonic shortening of the fold on the response of a representative three-layer (ductile, brittle, ductile) two-dimensional system. The model uses large deformation frictional contact mechanics to capture the response of existing fractures and slip along bedding surfaces, and considers both elastic and elastoplastic layer properties. The computational results demonstrate the relationships among overall configuration of the multilayer, slip on bedding surfaces, and the sequence and mode of deformation (opening versus shearing) of bed-perpendicular fractures. We show that fractures located in the hinge are mainly reactivated as joints and that those in the forelimb are predominantly reactivated as thrust faults. A flexural-slip mechanism develops during folding when the layers bounded by frictional bedding surfaces have similar stiffnesses. In contrast, when the difference in the layer stiffnesses is significant (softer outer layers) the deformation is accommodated within the softer units without exceeding the frictional strength of the bedding surfaces. A reduction of the middle layer thickness from 100 m to 10 m has a minor quantitative effect on the slip along the bedding surfaces. We compare the numerical results with fracture data collected at Sheep Mountain Anticline, and discuss the similarities and differences between the field observations and the model results.

1. Introduction

Folds in sedimentary rocks result from a number of mechanisms, including buckling due to lateral tectonic compression and slip on thrust faults in the underlying strata (e.g., Johnson, 1977; Johnson and Fletcher, 1994; Erickson and Jamison, 1995; Bobillo-Ares et al., 2000; Mühlhaus et al., 2002; Sanz et al., 2007). Displacements of folded strata may be a significant fraction of the wavelength and the kinematics may include significant rigid-body translations and rotations, as well as considerable straining and/or fracturing. Understanding the physics responsible for folding and fracturing is critical to the planning and management of activities that have significant economic impact because folds are common traps for fluids such as water and hydrocarbons. The permeability and flow paths of fractured aquifers and reservoirs depend largely on the geometry and hydraulic conductivity of the fracture network. Fractures in both hydrocarbon reservoirs and groundwater aquifers are known to form important conduits for fluid flow (National Research Council, 1996; Coward et al., 1998; Haneberg et al., 1999). In the context of folds, fractures not only help to charge the rock volume with fluids (Aydin, 2000), they can also rupture the seal and destroy the trapping potential (Smith, 1966; Jones et al., 1998).

Much progress has been made to understand how bedding-surface faults and fractures develop during folding (e.g., Wickham et al., 1982; Fischer and Wilkerson, 2000; Erickson et al., 2001; Guiton et al., 2003a,b; Casey and Butler, 2004; Maerten and Maerten, 2006). Fractures initiate from stress concentrations at flaws and fracture tips (Griffith, 1921; Lawn and Wilshaw, 1975; Pollard and Aydin, 1988; Renshaw and Pollard, 1994; Anderson, 1995), and subsequent reactivations take place as resolved stresses overcome the fracture strengths. Bedding-surface faults initiate and propagate in flexural-slip folds (Behzadi and Dubey, 1980; Cooke and Pollard, 1997; Engelder and Peacock, 2001; Erickson et al., 2001) where shear stress overcomes the cohesion and frictional resistance to sliding. Therefore, understanding the stress

* Corresponding author. Tel.: +1 650 861 0687; fax: +1 650 725 9755.
E-mail address: pfsanz@stanford.edu (P.F. Sanz).

0191-8141/$ – see front matter © 2008 Elsevier Ltd. All rights reserved.
doi:10.1016/j.jsg.2008.06.002

distribution in folding strata in space and time is a prerequisite for evaluating slip on bedding surfaces and reactivation of fractures. Stresses that develop during folding are affected by the interaction between deforming rock layers with different mechanical properties (Treagus, 1988; Bai and Pollard, 2000; Bai et al., 2000; McConaughy and Engelder, 2001; Bourne, 2003), the interfacial condition of the layer boundaries and the presence or absence of bed-parallel slip (Pfaff and Johnson, 1989; Nino et al., 1998; Cooke et al., 2000; Couples and Lewis, 2000; Johnson and Johnson, 2000; Cooke and Underwood, 2001; Guiton et al., 2003a,b). In addition, the stress distribution will change over time as the fold amplifies, the bedding rotates (Fischer and Wilkerson, 2000; Engelder and Peacock, 2001), and early formed fractures rotate and/or reactivate (Cruikshank et al., 1991; Cruikshank and Aydin, 1995; Wilkins et al., 2001; Bellahsen et al., 2006).

We present results from a mechanical model that captures the evolution of slip and opening of bedding surfaces and pre-existing fractures during the formation of an asymmetric anticline using finite elements (FEM) and large deformation contact mechanics. Mechanical forward-modelling that follows the evolution of discontinuities in the displacement field are essential for making comparisons to structures that can be observed at the outcrop scale. We build on the work of Guiton et al. (2003a,b) who studied the chronology of fracture activation in folded structures using finite elements and a constitutive model for rock that accounts for the presence of inherited fracture sets. In their models, the fractured rock mass is considered to be a continuum, hence the slip or opening of fractures is captured in a diffuse manner. In contrast, we address the discontinuities across bedding surfaces and fractures in a discrete manner. Therefore, the continuum description applies not to the fold scale, but to the regions bounded by bedding surfaces and fractures (i.e., discontinuities). Given the difference between the fold scale and fracture scale, and computational resources, we restrict the models to layer thicknesses and fracture spacings equal to or greater than 10 m, and to a three-layer composite. Therefore, the models do not explicitly capture the behavior of thinner beds and more closely-spaced fractures. Nonetheless model results provide insightful comparisons to field observations.

The finite-element models analyze representative bedding surfaces and fractures via contact mechanics. Large deformation contact kinematics is appropriate to use when the displacement field across an interface may be discontinuous, which is the case for fractures and bedding surfaces in flexural-slip folds. The application of large deformation frictional-contact models (Laursen, 2002; Wriggers, 2002) allows fractures and bedding-surface faults to be analyzed in the context of large displacement fields during folding. Contact mechanics captures a normal discontinuity (gap), a tangential discontinuity (slip), or no discontinuity (stick or bonded) along a pre-defined interface. In this work, we use frictional contact mechanics to investigate (i) slip or gap on fractures, (ii) slip along bedding surfaces, and (iii) to apply boundary conditions on the multilayer model.

Recent studies (Bellahsen et al., 2006; Fiore, 2006) characterize and consider the role of different fractures sets in the structural interpretation of Sheep Mountain Anticline (SMA), Wyoming. We build on this work and use the SMA fold geometry and a set of prefolding, bed-normal fractures (Set I) as a basis for the model. Thus, one objective of this paper is to model the kinematic aspects of inherited fractures, such as Set I in SMA (Bellahsen et al., 2006; Fiore, 2006), throughout the evolution of the anticline, and to compare the model results to the field observations. The models are a gross idealization and simplification of nature in terms of two dimensionality, number and thickness of layers, constitutive models of rock and interfaces, and spatial density and number of fracture sets. Therefore, a second objective is to describe, for its heuristic value, the mechanical behavior of such a fractured, multilayered system subject to asymmetric folding. We study the

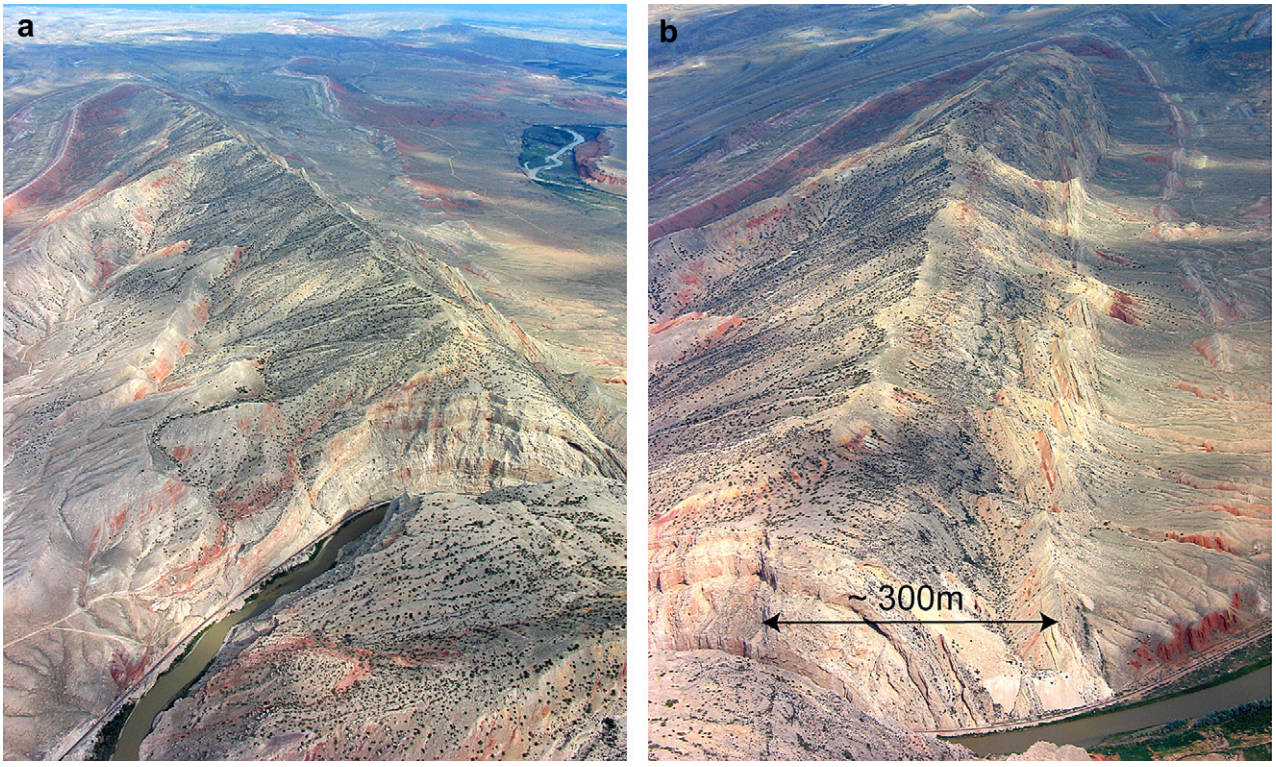

Fig. 1. Aerial views of Sheep Mountain Anticline looking (a) north along the gently-dipping backlimb and (b) northwest along the steeply-dipping forelimb. Bighorn River canyon is in the foreground. Approximate distance from the river cut to the nose of the fold is 6 km.

influence of mechanical stratigraphy, slip on bedding surfaces, and the magnitude of tectonic contraction on fracture development. In this work, *mechanical stratigraphy* refers to the variation of rock-layer thickness (perpendicular to bedding) and their mechanical properties.

First we present a summary of fracture data from SMA and its interpretation by Bellahsen et al. (2006). Then, we develop numerical models to study fracture evolution during folding. After describing the numerical results, we compare the field observations with the model results, and discuss the similarities and differences along with the limitations of the model. Finally, we summarize the findings and outline their implications for future work.

2. Geologic setting and fracture data

Sheep Mountain Anticline, located on the eastern edge of the Bighorn Basin, Wyoming, is a well known NW–SE trending, asymmetric Laramide fold (Fig. 1). The Laramide orogeny was characterized by a NE–SW compression (Engebretson et al., 1985; Bird, 2002). The Bighorn River cuts the anticline normal to the fold axis, providing exposure of rock strata in the fold core. The fold overlies and formed in association with slip on a fault that is interpreted as a SW-dipping thrust (Hennier and Spang, 1983; Forster et al., 1996; Stanton and Erslev, 2004). The forelimb of SMA dips between 40° and 90° northeast. This dip is steeper in the central part of the fold and shallower near the fold noses. Bedding dips are between 10° and 40° southwest in the backlimb. Bed-parallel slip, evidenced by slickensides and related minor thrusts, indicates a component of flexural-slip folding with slip directions approximately normal to the fold axis (Hennier and Spang, 1983).

The sedimentary units above granitic basement rocks in the Bighorn Basin are approximately 3 km thick (Hennier and Spang, 1983; Rioux, 1994; Forster et al., 1996). Fig. 2 shows the formations that crop out at SMA. The oldest exposed unit is the Lower Mississippian Madison Limestone which has an approximate thickness of 230 m (Fig. 2). Above this unit, the Mississippian Amsden Formation (35 m thick) consists of crossbedded quartz arenites, siltstones, sandstones, shales and carbonates. The Amsden Formation is overlain first by sandstones, shales, and carbonates topped by quartz arenites of the Upper Mississippian Tensleep Formation (29 m thick). The Permian Phosphoria Formation is next at about 70 m thick with predominantly siltstones and shales overlain by thick carbonates. Above these formations lies the Triassic Chugwater Formation, the youngest unit exposed at SMA,

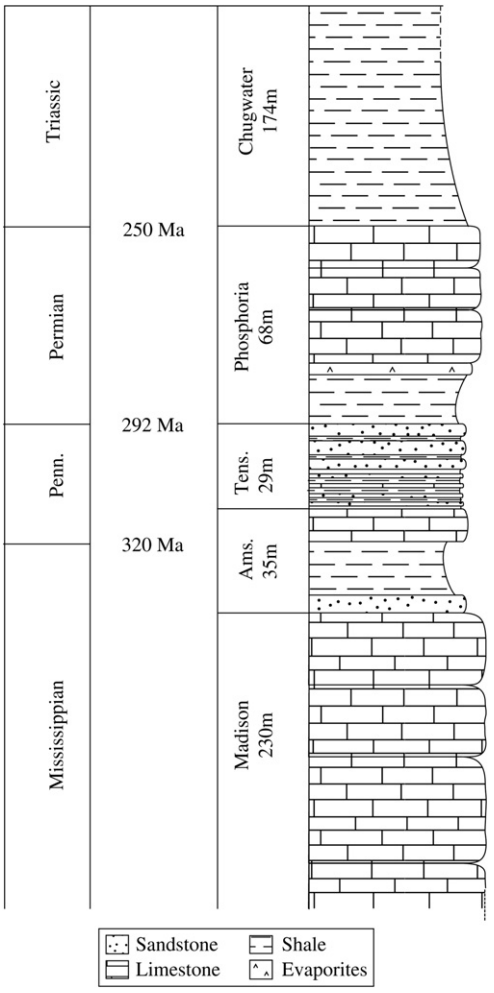

Fig. 2. Stratigraphy exposed at Sheep Mountain (after Ladd, 1979). Abbreviations: Pennsylvanian (Penn.), Amsden (Ams.), Tensleep (Tens.). Reproduced from Bellahsen et al. (2006).

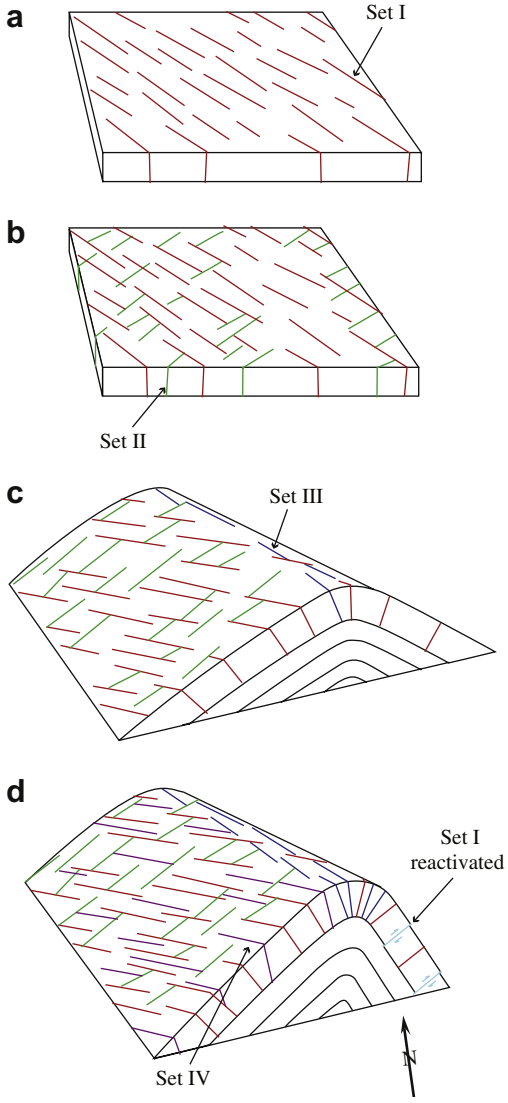

Fig. 3. Schematic representation of the fracturing history at Sheep Mountain Anticline (from Bellahsen et al., 2006). (a) Set I (red); (b) Set II (green); (c) Set III (blue); (d) vertical Set IV (purple) parallel to Set I fractures in the backlimb, and Set I fractures are reactivated in the forelimb as reverse faults.

which is approximately 170 m thick with sandstones and shales. Given the complexity of this stratigraphy, and the current limitations of FEM models, we chose to model a three-layer composite of initially constant thickness that represents presumed ductile-brittle–ductile sequences such as shale–sandstone–shale or shale–limestone–shale. This idealized configuration does not explicitly represent any specific formation or part thereof, but we suggest it does provide an analogous mechanical stratigraphy, while honoring overall structural geometry of the natural example.

Fracture field data were previously collected north of the Bighorn River (Bellahsen et al., 2006; Fiore, 2006). Sandstones were sampled from the Amsden Formation in the hinge and from the Tensleep Formation in the limbs. Four fracture sets were identified in SMA based on orientation data and deformation mode (Fig. 3). Reported fracture orientations for Sets I, II, and III are unfolded relative to bedding. Reported orientations for Set IV are present orientation. Set I fractures strike 110°, oblique to the fold trend, and are interpreted as a regional fracture set that was present before the Laramide anticline and related stress field. Set II, joints striking 045° and present in the hinge and backlimb, are interpreted as related to the NE-oriented Laramide compression just prior to and during initial anticline growth. Joints striking 135° (Set III), parallel to the fold trend, are found mainly within the hinge and are interpreted to have formed in response to flexural stresses during folding. Set IV, vertical joints oblique to the fold axis and striking 110°, developed in the backlimb during a late stage of folding. Bellahsen et al. (2006) inferred that the fracture patterns indicate fixed-hinge folding with little lateral propagation of the underlying thrust fault and the anticline. Set I fractures, found throughout the fold and perpendicular to bedding, may have initiated as shear fractures or deformation bands, or as joints that subsequently were sheared. In the forelimb, these fractures were reactivated as late-folding thrust faults (Fig. 3d), but in the backlimb they show no kinematic evidence of thrust faulting (Bellahsen et al., 2006). There is well-documented evidence for strike-slip faulting of Set I fractures in the backlimb (Fiore, 2006), which relates to the three-dimensional nature of SMA and cannot be addressed by our two-dimensional models.

3. Methodology

We investigate folding and the evolution of existing fractures using an innovative method. This methodology requires the use of state-of-the-art computational mechanics tools as well as the development of mathematical models based on continuum and contact mechanics. The mechanical models are two-dimensional (plane strain) and involve a composite of three individual layers of initial constant thickness with distinct constitutive properties. A representative domain contains a middle layer with bed-perpendicular fractures sandwiched between two continuous layers (Fig. 4). The trio can bend, stretch, or shorten into prescribed geometric configurations. The model allows slip and/or opening on fractures and bedding surfaces and hence, the need for frictional contact constraints along these interfaces. The reactivation of discontinuities in both sliding and opening is modeled using non-

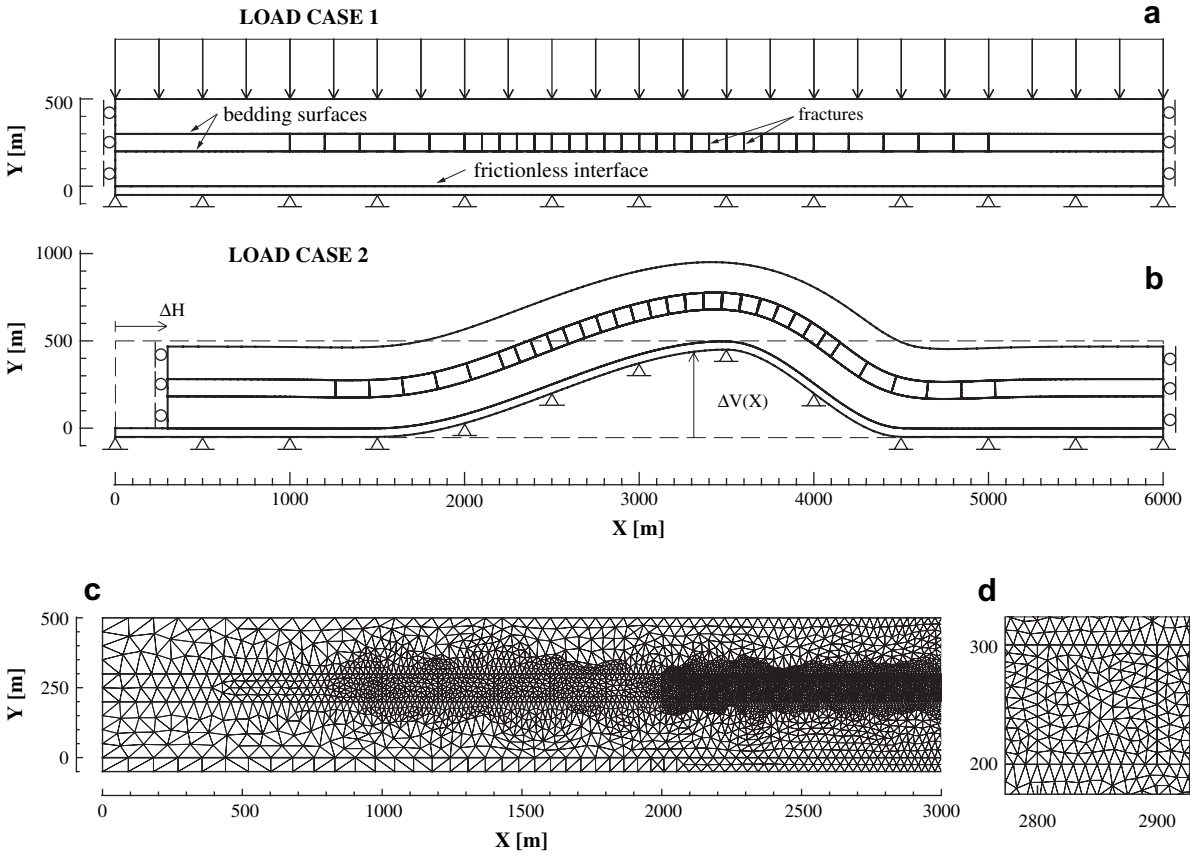

Fig. 4. Model configuration and finite-element mesh. (a) Overall geometry of the undeformed configuration (load case 1); the model has 31 originally-vertical fractures and 3 originally-horizontal contact surfaces; the circles along the vertical boundaries are roller supports (constraint horizontal displacements) and the triangles along the bottom boundary are pin supports (constraint horizontal and vertical displacement). (b) Overall geometry of the deformed configuration; the dashed lines illustrates the undeformed configuration; ΔH and $\Delta V(X)$ are the horizontal and vertical displacements imposed from the left and bottom of the model respectively. (c) Finite element mesh of model's left-half. (d) Close-up view of the inner-layer finite element mesh.

linear contact mechanics. The model uses nonlinear finite element methods, considering both geometric and material nonlinearities.

A regularized Coulomb friction law simulates the mechanical response of the interfaces (Laursen and Simo, 1993; Wriggers, 1995, 2002). Each contact surface has three mechanical parameters: a normal elastic stiffness ε_N, a tangential elastic stiffness ε_T, and a sliding friction coefficient μ. The tangential elastic stiffness is the regularization parameter, which for $\varepsilon_T \to \infty^+$ yields the classical Coulomb law that predicts a perfect stick-slip motion. Frictional slip is path-dependent in nature and its evolution requires the integration of the constitutive law in finite steps. The integration is performed by a return-mapping algorithm in a similar way to a non-associative plasticity model (Wriggers, 2002). We discretize the interfaces with node-to-segment contact elements (Laursen and Simo, 1993; Wriggers, 1995, 2002) that allow any node on the interface to slide over the entire contact area.

Tracking the evolving configurations of the layers, the discontinuities, and their structural features is a challenging aspect of the modeling. The most suitable approach for capturing finite deformation effects in structural geology is to adopt a fully Lagrangian description of the motions (Crook et al., 2006a,b). We implemented the constitutive models and finite deformation contact elements in a Fortran non-linear finite element code based on such a Lagrangian description. The fully implicit numerical implementation includes a consistent linearization of the weak form of the linear momentum balance to enable optimal convergence for Newton–Raphson iterations, which appears to be essential for the general robustness of implicit finite-element techniques (Simo and Taylor, 1985; Borja et al., 2003). A more detailed discussion of the mechanical framework and of the numerical implementation is in Sanz et al. (2007).

4. Mechanical model

The finite element models consist of a three-layer composite overlying a sliding interface (Fig. 4). To reduce the number of elements, and thus the computational time, the spacing of the fractures and the size of the elements is increased away from the areas of interest (i.e., the anticlinal region). The finite element discretization led to almost 13,000 constant strain triangular elements and 1000 contact elements. The mesh is originally 6000 m wide (L_o). The middle layer is 100 m thick (H_m) and the two outer layers are 200 m thick (H_o), so the total undeformed thickness of the composite is 500 m. At the bottom of the three-layer composite an auxiliary layer with a frictionless interface is used to impose displacement boundary conditions that deform the composite into a representative current configuration of the Sundance Formation on a cross section near the Bighorn River canyon (Forster et al., 1996; Bellahsen et al., 2006).

A total of 31 vertical fractures numbered in ascending order, left to right, are distributed along the middle layer of the composite (Fig. 4). The spacing of the fractures throughout the anticlinal region is 100 m. Each fracture transects the entire layer and is capable of slip at a constant coefficient of friction $\mu = 0.58$ (Byerlee,

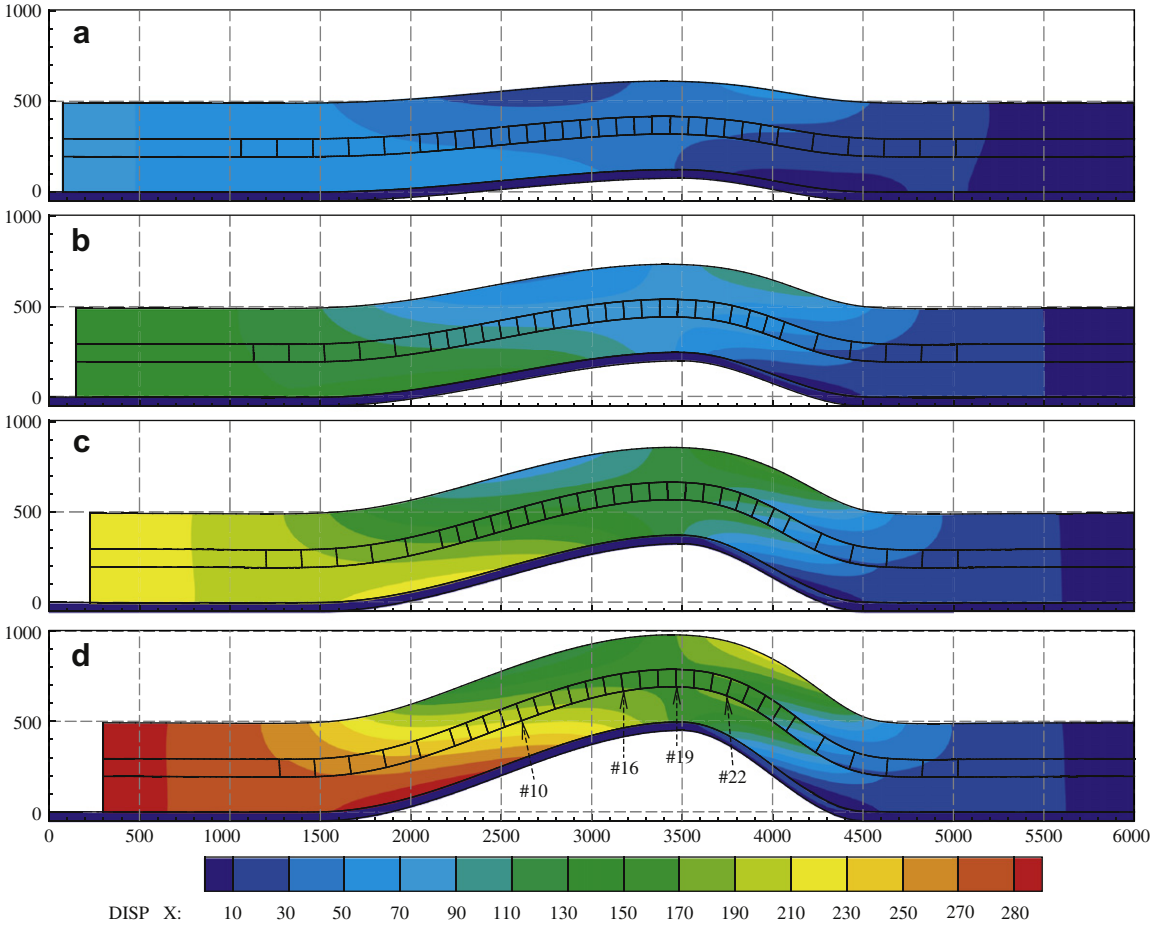

Fig. 5. Progressive deformation for folding model with parameters $r = 1$ and $\chi = \Delta H/\Delta V = 0.6$. Discontinuous contours indicate slip along interfaces with displacements shown in true scale. Black lines indicate contact interfaces (fractures and bedding surfaces). Model configuration is shown after a total horizontal displacement of the left vertical side of (a) 75, (b) 150, (c) 225, and (d) 300 m. Dashed arrows indicate fracture numbers, horizontal coordinates, vertical coordinates, and horizontal displacement (DISP X) bar scale in meters.

1978; Carmichael, 1982) that corresponds to a residual friction angle of 30°. The two surfaces are pinned at fracture tips, so opening and slip are precluded at the bedding surfaces. A stress singularity does not exist at the fractures tips in the numerical solution.

The unit weight of the rock layers is assumed to be 26 kN/m^3, which is as an average value of sedimentary rocks from Carmichael (1982). The top surface of the composite is subjected to a vertical traction of 40 MPa approximating the lithostatic loading during folding. The onset of the Laramide orogeny in the Bighorn Basin area occurred during the late Cretaceous, so we assume that the 2.0 km of post-Pennsylvanian to Cretaceous sedimentary rock to be an approximate burial depth of the Pennsylvanian units during deformation (Rioux, 1958; Hennier and Spang, 1983; Forster et al., 1996). The vertical sides of the model are constrained with roller supports so no tangential tractions are imposed, but a uniform horizontal displacement may be prescribed to simulate the regional shortening during folding. The loading history consists of two stages: in the first (Fig. 4a), we apply the vertical load and the unit weight (load case 1: gravitational loads), and in the second (Fig. 4b), we simulate the folding by prescribing horizontal displacements to the left side and vertical displacements through the auxiliary layer at the bottom (load case 2: shortening and folding). As a simple first approximation to fold growth we assume that the vertical displacement of the model bottom boundary evolves self-similarly. To investigate the legitimacy of self-similar fold growth is beyond the scope of this work; however, it has been addressed in other studies (e.g., Fischer and Woodward, 1992; Fisher and Anastasio, 1994).

To limit the number of simulations only a subset of possible variables were considered: the ratio of uniform horizontal contraction to maximum vertical displacement of the composite; the ratio between the deformation moduli of the middle and outer layers; and the tangential response of the bedding surfaces as no-slip or bonded versus a weaker frictional slip behavior with a friction coefficient $\mu = 0.58$. Given the complex stratigraphy at SMA, we fix the deformation modulus of the middle layer and change the deformation modulus of the outer layers to evaluate the effect of different mechanical stratigraphy on the system response. The term *modulus of deformation* signifies that its value accounts for both elastic and permanent deformation (Goodman, 1989). The mechanical properties we use for the middle layer are: deformation modulus $E_m = 2000$ MPa and Poisson's ratio $\nu = 0.25$. The outer layers have the same Poisson's ratio and deformation modulus E_o, ranging from 200 MPa to 4000 MPa. The ratio of deformation moduli, $r = E_m/E_o$, characterizes the variation of the rock stiffness between the middle and outer layer. The deformation moduli approximate the mechanical behavior of the intact rock and fractures not explicitly incorporated into the model, so these moduli are smaller than those of the intact rock. The difference between the Young's modulus of the intact rock and the modulus of deformation of the rock mass is significant when the rock is highly fractured (Bieniawski, 1978) due to the existence of weak discontinuities and

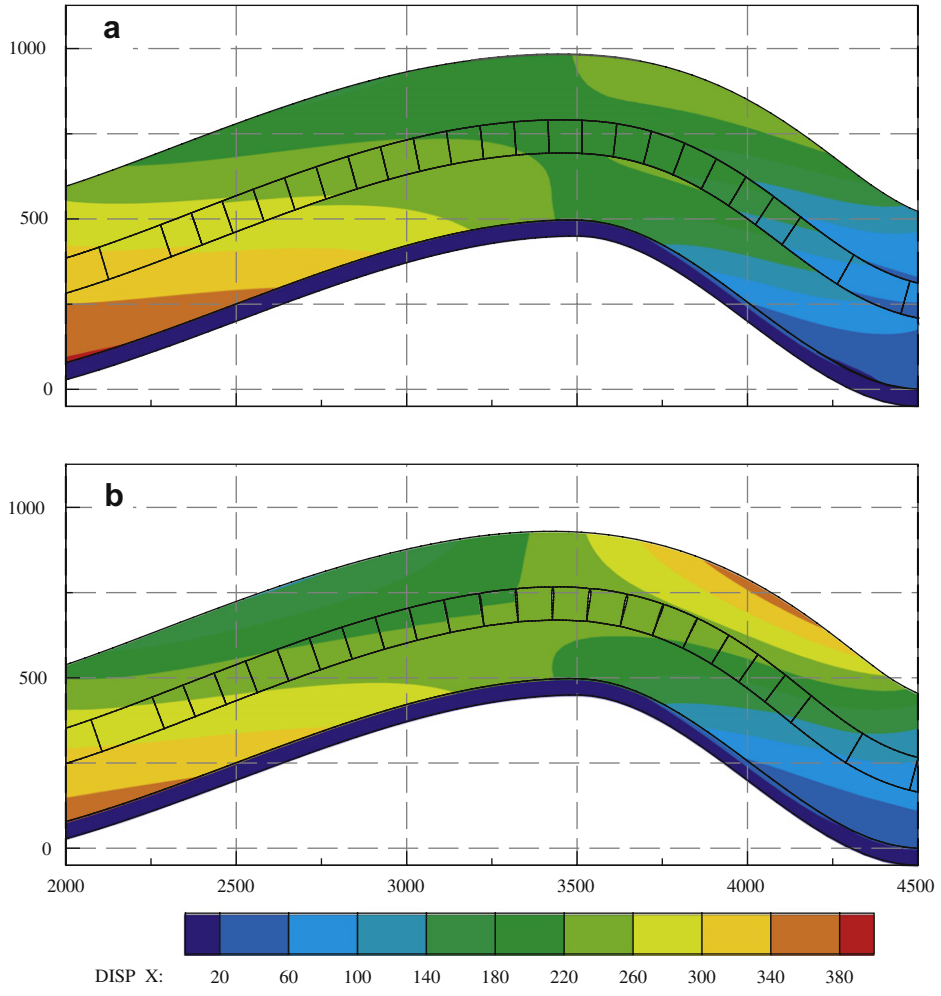

Fig. 6. Deformed configuration after a horizontal contraction of 400 m ($\varepsilon = 6.7\%$; $\chi = 0.8$). (a) Stiff outer layers ($r = 1$). (b) Soft outer layers ($r = 10$). Solid black lines denote contact interfaces (fractures and bedding surfaces). Horizontal coordinates, vertical coordinates, and horizontal displacement (DISP X) bar scale in meters.

permanent deformation localized along them. For this reason the strength and stiffness of rock masses typically decreases with increasing sample size (Jaeger and Cook, 1969; Strayer and Hudleston, 1997; Pollard and Fletcher, 2005).

A reasonable first approximation for the pre-folding geometry of the sedimentary units is that they were horizontal, planar, and had constant thickness. The post-folding geometry of selected bedding surfaces along the area of interest is available from structure contour maps of SMA (Forster et al., 1996; Bellahsen et al., 2006). Here, we use the deformed (current) configuration of the Sundance Formation to constrain the base of the composite along the anticlinal region of the fold. Although this configuration of the Sundance Formation is taken as a given, the actual displacement distribution and the deformation path are unknown. Given the aforementioned constraints, we use an auxiliary layer and contact mechanics to prescribe the desired configuration of the bottom surface without imposing capricious or unrealistic displacements. As we deform the auxiliary layer, the bottom boundary of the domain will slide along the frictionless interface and deform into the prescribed geometric configuration (Fig. 5). Thus, the unknown vertical and horizontal displacements of the bottom surface are not imposed directly, but the desired configuration is attained. The prescribed uplift at the bottom boundary is the result of regional contraction and slip along an underlying thrust fault. The distance from the idealized layers to the tip of that fault is unknown, but it is below the area of interest, and is not incorporated in the model. The displacements attained by the composite are constrained by the mechanical properties of the layers, the interfacial conditions, and the conservation of mass and momentum.

The deformation paths followed by particles in the composite are strongly dependent on the ratio of horizontal shortening to vertical uplift. The maximum vertical displacement of the base of the composite at the end of the simulation, ΔV, is 500 m (e.g., see Fig. 5d). We conducted a sensitivity analysis to better understand the effect of tectonic shortening (i.e., the horizontal displacement boundary condition imposed on the left side of the composite). We applied uniform shortening displacements ΔH of 200 m, 300 m, and 400 m, yielding overall contractions, $\varepsilon = \Delta H/L_o$, of 3.3%, 5.0%, and 6.7%, respectively. Resulting ratios of horizontal displacement and maximum vertical uplift, defined as $\chi = \Delta H/\Delta V$ are 0.4, 0.6, and 0.8, respectively. In any particular simulation, the ratio between the horizontal displacement and maximum vertical uplift remains constant.

The mechanical model presented above is complex despite the assumption of a simple constitutive law for the non-fractured media of the middle layer (i.e., elastic). We choose to emphasize the importance of structural discontinuities (fractures and bedding surfaces) on the behavior of this layer (Müller, 1979; Goodman, 1989) by considering that inelastic deformation of the intact rock between fractures is negligible. In doing so, we anticipate that all permanent deformation will be localized along these structural discontinuities (bed-perpendicular fractures and beddings surfaces). The outer layers are treated as both elastic and elastoplastic to evaluate the effects of plasticity in the ductile members of the composite.

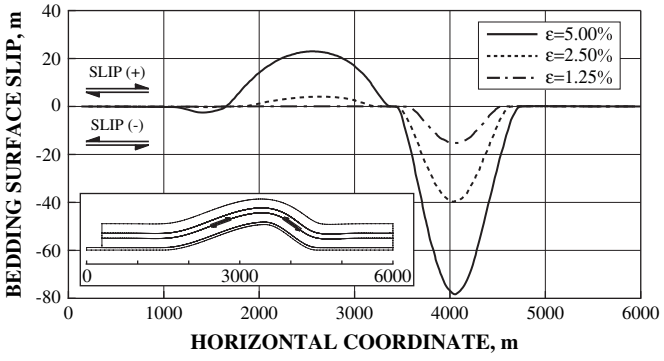

Fig. 7. Evolution and spatial variation of slip along bottom bedding surface; $r = 0.5$; $\chi = 0.6$. Inset shows location and sense of slip along the fold. Slip is right-lateral (positive) in the backlimb and left-lateral (negative) in the forelimb.

5. Numerical results

To gain insight into the chronology and mode of fracture reactivation during folding, we conducted forty simulations for different combinations of mechanical stratigraphy (thickness and mechanical properties of the rock layers), overall contraction of the fold, and strength of bedding surfaces.

5.1. Effect of bed-parallel slip

Of interest here is the relation between overall deformation and mechanical stratigraphy with bed-parallel slip. Viewed at successive stages of a simulation (e.g., Fig. 5), bed-parallel slip along the limbs increases gradually, and is greater in the forelimb because slip approximately scales with bed dip (Ramsay, 1974; Suppe, 1985; Behzadi and Dubey, 1980; Horne and Culshaw, 2001). In this simulation (Fig. 5), the same mechanical properties were used for all layers ($r = 1$); however, as the fold amplifies and fractures reactivate, the apparent stiffness of the middle layer decreases because inelastic deformation is localized along the fractures. Because the outer layers are relatively stiffer, slip on bedding surfaces plays a more prominent role in fold development.

For comparison, consider the deformed central section of an asymmetric anticline after a horizontal contraction of 400 m ($\varepsilon = 6.7\%$, $\chi = 0.8$) when the outer and middle layers have the same stiffness ($r = 1$, $E_o = 2000$ MPa) and when the outer layers are considerably softer than the middle layer ($r = 10$, $E_o = 200$ MPa). Folding in the first case (Fig. 6a) leads to layer-parallel slip at the interfaces that initiates in the forelimb at an early stage of the deformation ($\varepsilon = 0.9\%$), while in the backlimb, the slip starts much

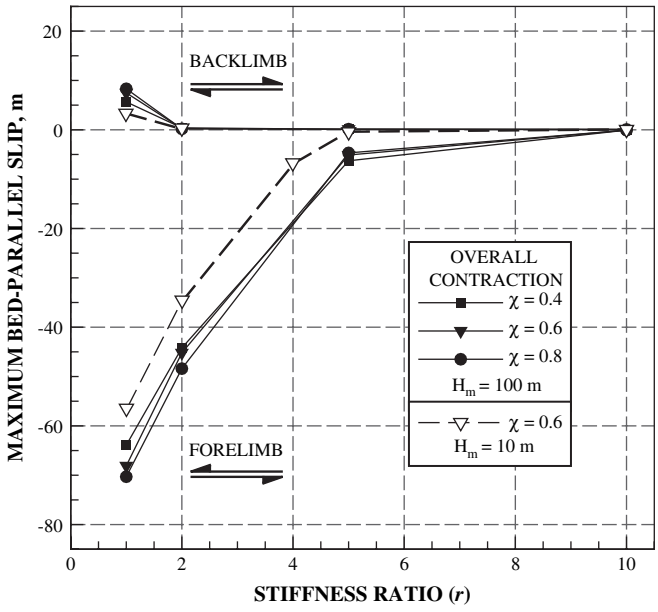

Fig. 8. Maximum and minimum slip on the bedding surface located along the bottom boundary of the middle layer for middle layer thickness $H_m = 100$ m (solid symbols) and $H_m = 10$ m (open symbols). Slip is right-lateral (positive) in the backlimb and left-lateral (negative) in the forelimb.

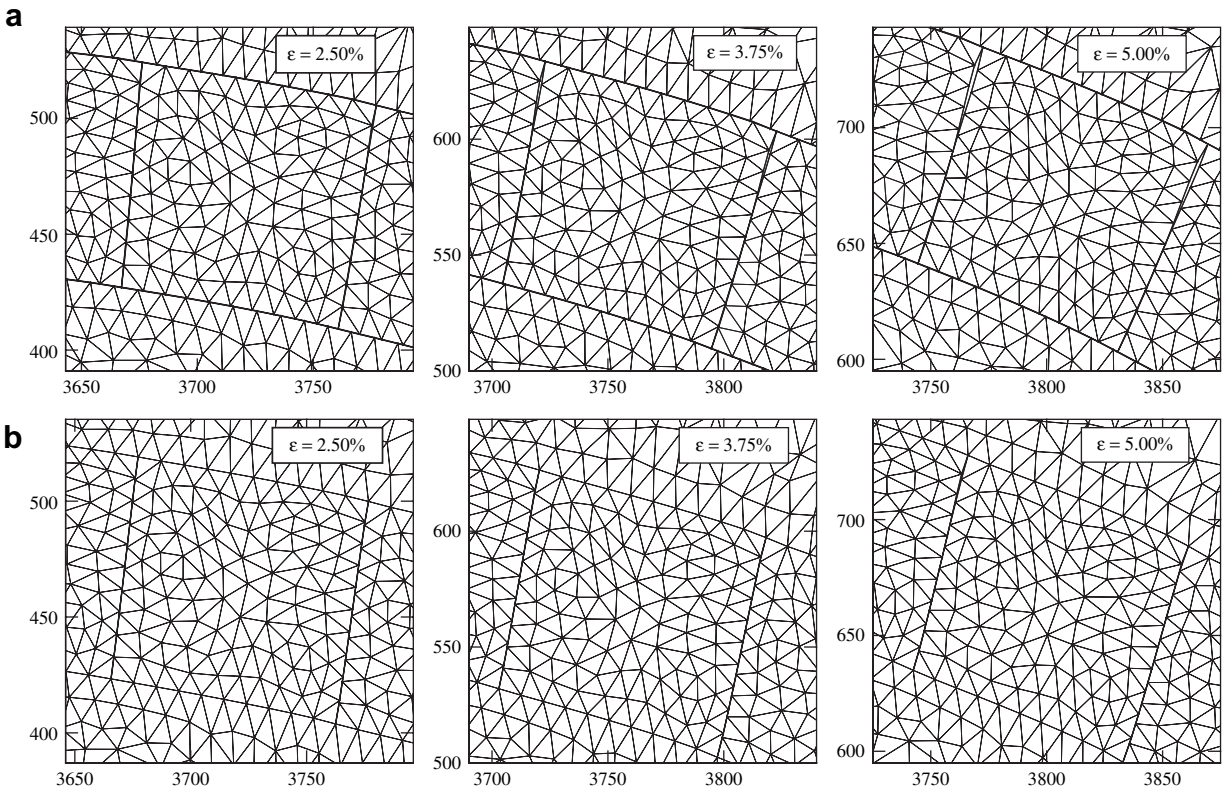

Fig. 9. Snapshots of deformation in the forelimb showing fractures #22 and #23 ($r = 1$, $\chi = 0.6$, and $H_m = 100$ m): (a) frictional bedding surfaces; (b) bonded bedding interfaces. Horizontal and vertical coordinates in meters.

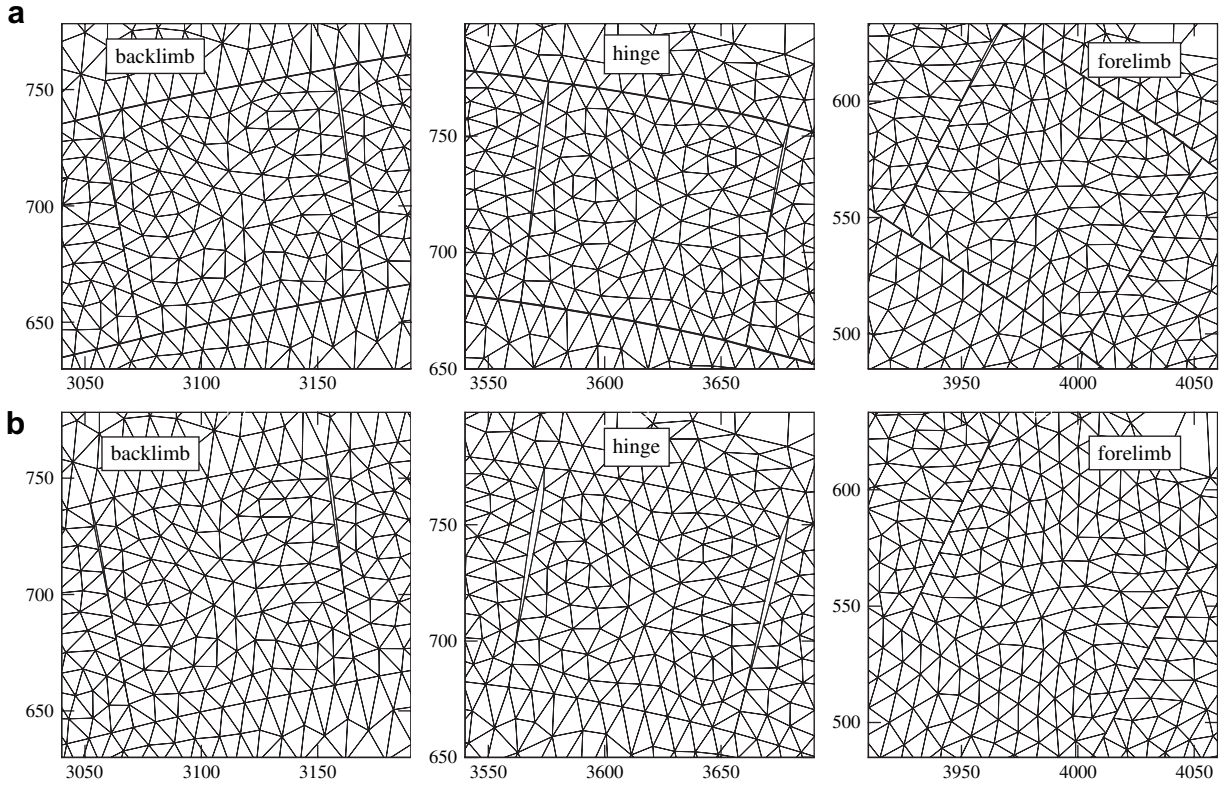

Fig. 10. Reactivation of backlimb (#15 and #16), hinge (#20 and #21), and forelimb fractures (#24 and #25) after horizontal contraction of 300 m ($\varepsilon = 5.0\%$); $r = 2$; $\chi = 0.6$; $H_m = 100$ m. (a) Frictional bedding interfaces. (b) Bonded bedding interfaces. Horizontal and vertical coordinates in meters.

later ($\varepsilon = 4.4\%$). With the reduction of the outer layer's stiffness (Fig. 6b), a no-slip (bonded) condition prevails along the fold limbs giving rise to a folding mechanism akin to flexural flow (Ramsay, 1974): the outer layers deform, in this case elastically, rather than slip developing along the bedding interfaces.

Bed-parallel slip always initiates near the middle of each limb, starting on the forelimb, and spreading laterally in both directions (Fig. 7). This result agrees with previous numerical (Erickson et al., 2001) and experimental results (Kuenen and de Sitter, 1938) which demonstrate that bedding-parallel slip initiates at the inflection of limbs during folding. The evolution and spatial distribution of the slip on the upper and lower interfaces of the middle layer are similar. The maximum slip along the backlimb is slightly greater (about 10%) on the upper boundary than on the lower boundary. However, in the forelimb bed-parallel slip is greater by about 10% on the bottom interface than the upper.

The slip sense along the bedding surfaces is right-lateral in the backlimb and left-lateral in the forelimb (Figs. 7, 8). If the outer layers are softer (i.e., greater r), flexural slip is less important. Moreover, if the stiffness ratio is great enough, a no-slip condition develops, first on the backlimb (for $r > 2$) and then on the forelimb (for $r \geq 5$) because the softer units accommodate the deformation such that the resolved shear stress does not exceed the frictional strength of the bedding interfaces.

A reduction of the middle layer thickness has a minor quantitative effect on the bedding-surface slip. Here, the thickness of the middle layer is reduced along with an increase in the thicknesses of the outer layers, so the total thickness of the composite (500 m) is unchanged. Bedding slip decreases in magnitude as the middle layer thickness is reduced from 100 m to 10 m (Fig. 8). However, the difference is less than 20% at most for an order of magnitude reduction in the middle layer thickness. In contrast, an order of magnitude increase in the stiffness ratio decreases the maximum slip on the forelimb from about 60 m to zero. The no-slip condition is obtained at somewhat lesser stiffness ratios for the thinner middle layer.

5.2. Reactivation of bed-perpendicular fractures

For the layer-normal fractures in the middle layer, the mesh is originally conforming, so that any misalignment between nodes along the contacts during deformation is an indication of tangential or normal separation (shearing or opening) (e.g., Figs. 9 and 10). Fractures #22 and #23, which are in the forelimb but close to the hinge (Fig. 9a), are reactivated first in shear ($\varepsilon = 0.7\%$), and as slip evolves, they open on the upper third of the fracture ($\varepsilon = 2.4\%$). If bed-parallel slip is precluded (bonded bedding surfaces), a flexural flow-like mechanism is forced, and the middle layer is sheared more significantly and bed-normal fractures accommodate greater slip (Fig. 9b). By comparing Fig. 9a and b ($r = 1$ and $\chi = 0.6$) for the same overall horizontal shortening (equal ε), slip on forelimb fractures is greater but opening is less when slip is precluded on bedding interfaces.

For the bed-normal fractures in the middle layer opening-mode deformation prevails in the hinge region and a thrust-shearing mode prevails in the limbs (e.g., Fig. 10). Shear reactivation of fractures has greater displacement in the forelimb than the backlimb due to the steeper bedding dips in the forelimb. For the same reason, fracture reactivation occurs first in the forelimb, later in the backlimb, and then the hinge. Fracture opening in the hinge and shearing in the limbs are greater when slip is not permitted along the bedding interfaces (Fig. 10b). The fracture evolution is usually characterized by two stages: an initial stick condition (elastic response) followed by slip (inelastic response) according to the Coulomb friction law. A third stage is observed in some fractures (mainly along the forelimb) that experience an opening mode after shearing.

The sequence of reactivation is to some extent different in the case of strong (or bonded) bedding surfaces. The fractures are first reactivated in the forelimb, then in the hinge, and finally in the backlimb. The mechanics of reactivation not only varies across the fold (Fig. 10), but also changes along the same fracture as the fold evolves (Fig. 9). In the limbs, fracture slip initiates on the upper

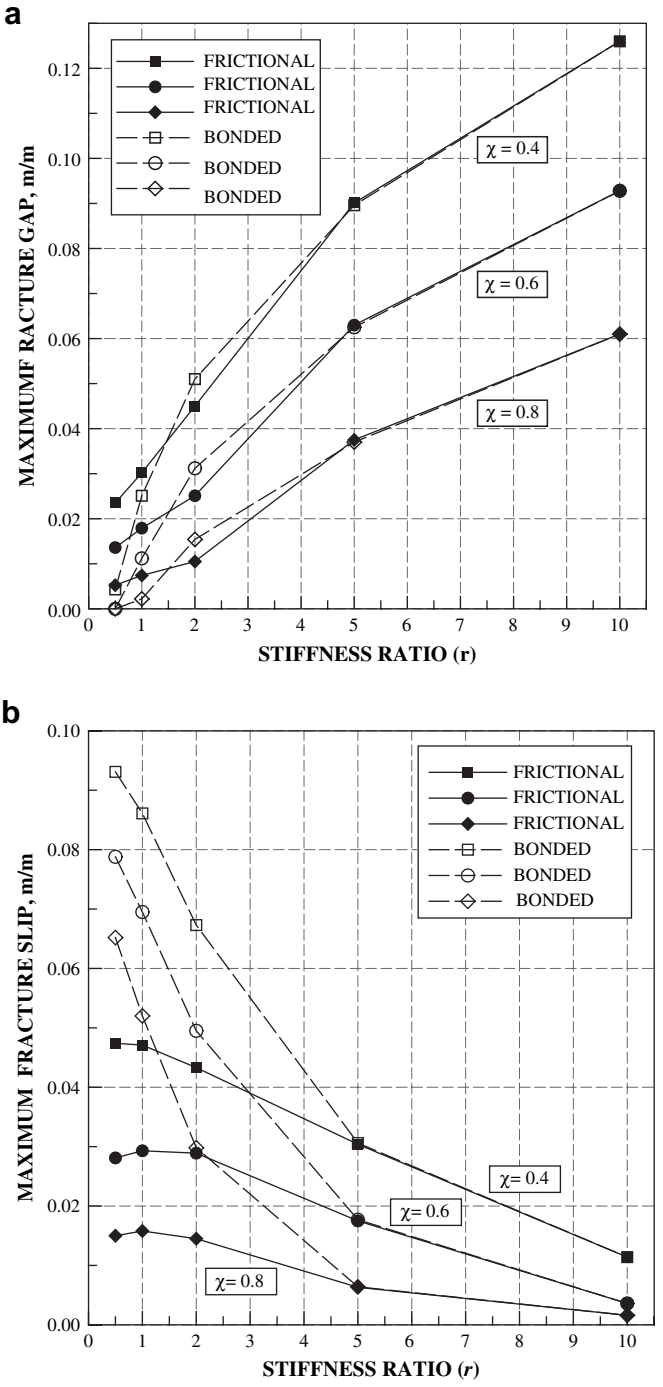

Fig. 11. (a) Maximum fracture-gap per meter (normalized) occurring in the hinge as a function of the stiffness ratio, r. (b) Maximum fracture-slip (normalized) occurring in the forelimb as a function of r. Solid lines correspond to frictional bedding surfaces; dashed lines with open symbols correspond to bonded bedding surfaces. The maximum gap and slip of a single fracture are normalized by the original distance between fractures (100 m).

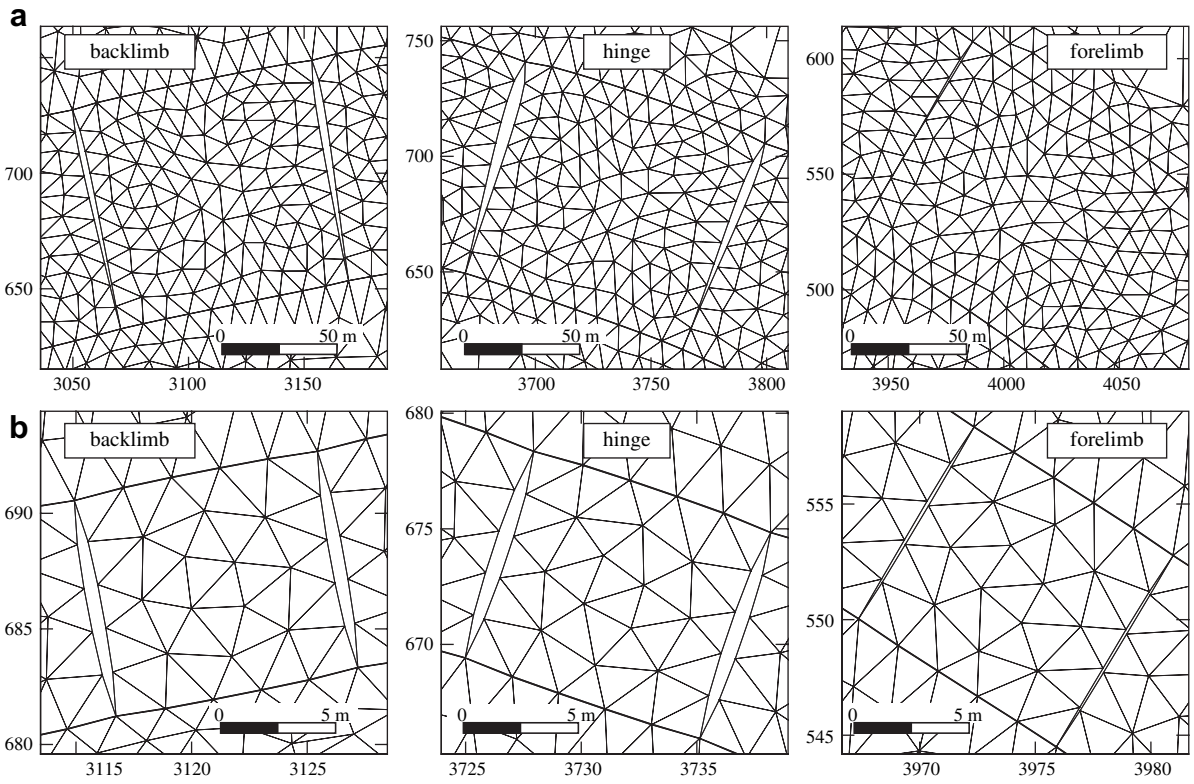

Fig. 12. Reactivation of backlimb (#15 and #16), hinge (#21 and #22), and forelimb fractures (#24 and #25) after a horizontal contraction of 300 m ($\varepsilon = 5.0\%$); $r = 5$; $\chi = 0.6$. (a) Middle layer thickness $H_m = 100$ m. (b) Middle layer thickness $H_m = 10$ m. Horizontal and vertical coordinates in meters. Thicker lines denote contact interfaces (fractures and bedding surfaces).

section of the fractures and progresses downward towards the lower section because the normal compressive stress is greater toward the concave side of anticlinal layers.

Maximum opening of bed-normal fractures, which occurs in the hinge, increases for increasing softness of the outer layers (r increases) and as overall contraction decreases (χ decreases) (Fig. 11a). There is a tendency for bed-normal fractures to open in the hinge during folding. However, fracture opening is suppressed with bonded bedding surfaces, stiffer outer layers ($r = 0.5$), and significant overall contraction ($\chi = 0.6$ and $\chi = 0.8$) as shown in Fig. 11a.

Reactivation of model fractures as reverse faults occurs in both limbs, but at different times and with different magnitudes (Fig. 11b). At the completion of fold growth, predicted slip on the forelimb fractures is about twice that predicted for the backlimb. Also, as the stiffness ratio increases, slip on forelimb fractures decreases while opening of hinge fractures increases (Fig. 11). If sliding occurs along the bedding surfaces for smaller stiffness contrast ($r < 5$), fracture slip is significantly reduced. Further, fracture slip is not substantially affected by the stiffness ratio for $r < 2$ if sliding occurs on bedding surfaces (Fig. 11b). Consequently, slip along bedding surfaces reduces the apparent stiffness of the outer layers. Finally, as the overall contractions increases (greater χ), the compression resolved on the fractures is greater so fracture opening and shearing are reduced.

Again, considering a case where the thickness of the middle layer is only $H_m = 10$ m vs. $H_m = 100$ m and $r = 5$, backlimb and hinge fractures are reactivated by opening while forelimb fractures are first sheared and then opened (Fig. 12). The spacing between fractures along the anticlinal region is the same as the middle layer thickness H_m for both models (10 m and 100 m respectively). The opening and slip developed along fractures scales with their height, such that decreasing the fracture height by an order of magnitude (from 100 m to 10 m) reduces the slip and gap by a similar factor. Bed-perpendicular fractures that are 100 m in height experience different displacement discontinuities near their ends, for example more opening near the top than near the bottom (Fig. 12a). When the middle layer thickness is reduced by an order of magnitude and fractures are only 10 m in height (Fig. 12b), the stress state across the fractures is more homogeneous and the displacement discontinuity is more symmetric.

5.3. Effect of bulk plasticity

For the model results described above, all permanent deformation and stiffness deterioration during folding is a result of

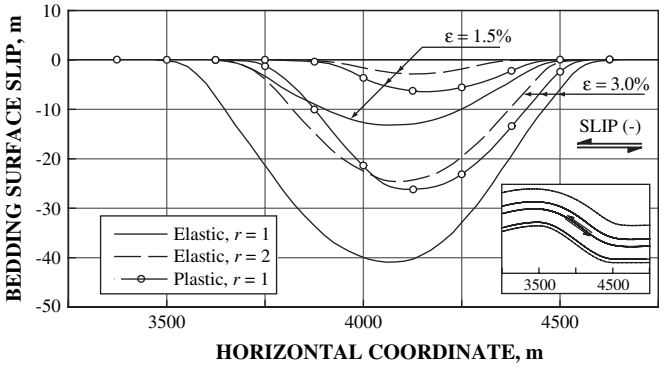

Fig. 13. Evolution and spatial variation of slip along the bottom bedding surface of the middle layer assuming elasticity and bulk plasticity for the outer layers; $\chi = 0.6$. Inset shows location and sense of slip (right-lateral) along the forelimb.

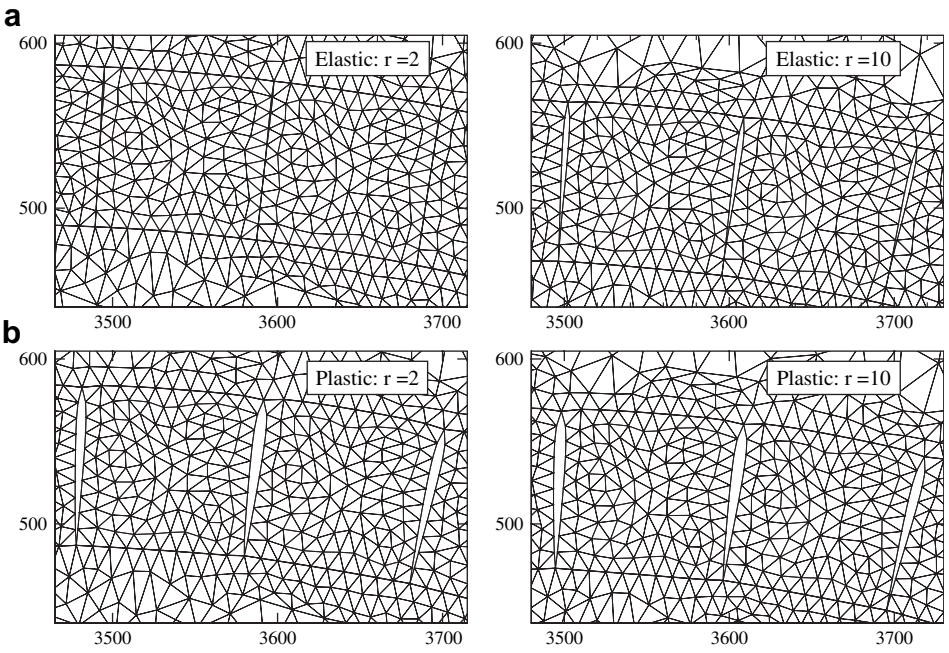

Fig. 14. Reactivation of hinge fractures (#20 to #22); $\varepsilon = 3.0\%$; $\chi = 0.6$; $H_m = 100$ m. (a) Outer layers with elastic rheology. (b) Outer layers with elastoplastic rheology. Horizontal and vertical coordinates in meters.

Fig. 15. Reactivated Set I fractures in the forelimb (looking N). Field photograph of thrust faults offsetting a sandstone bedding surface of the Tensleep Sandstone. Person on lower right for scale.

slip and/or opening at bedding surfaces and fractures. In this section, we consider the case of permanent deformations along the outer layers through elastoplastic deformation that may be more appropriate for ductile layers such as shales. We use an elastoplastic constitutive model to capture the effect of deterioration in the tangent stiffness with plastic deformation. The constitutive law is described by a three-invariant Matsuoka–Nakai yield criterion (Matsuoka and Nakai, 1974), a non-associative flow rule, and a non-linear hardening law. As with a Mohr–Coulomb model, the Matsuoka–Nakai yield criterion gives the same friction angle in extension and compression. This model material was incorporated into the fully implicit FEM program via multiplicative plasticity (Borja et al., 2003). We assume that the initial and final sizes of the yield surface correspond to friction angles $\phi_i = 15^\circ$ and $\phi_f = 34^\circ$ respectively (friction hardening), the dilatancy angle is $\psi = 12^\circ$, and the cohesion is 5 MPa. The elastic parameters, Young's modulus and Poisson ratio, are the same as those used above (i.e., Section 4). Note that these friction angles represent the bulk plasticity response of the outer layers (i.e., how fast the conical yield surface expands with the compressive mean normal stress), and do not describe the Coulomb-constrained friction along the discontinuities. In this analysis, we did not checked the solution for localized or diffuse instability such as shear banding or cataclastic flow (Borja, 2006).

Plasticity initiates in the upper parts of the outer layers in the hinge, where horizontal extension occurs due to layer bending, and advances downward as the fold develops. Model results show that plastic deformation along the outer layers is greater in the hinge than in the limbs, where the stress state is mostly dominated by shear stresses parallel to bedding. For this reason, and given that the friction angle of the bedding surfaces, $30^\circ = \tan^{-1}(\mu)$, is less than the friction angle of the outer layers, $\phi_f = 34^\circ$, the deformation along the limbs is mostly accommodated by bedding-surface slip rather than distributed plastic strains in the layers. Therefore, the stresses in the limbs are constrained by the Coulomb friction law along the bedding surfaces. As slip increases along the bedding surfaces, the necessity for plastic deformation in the adjacent layer decreases because the stresses are limited by the frictional strength of the discontinuities.

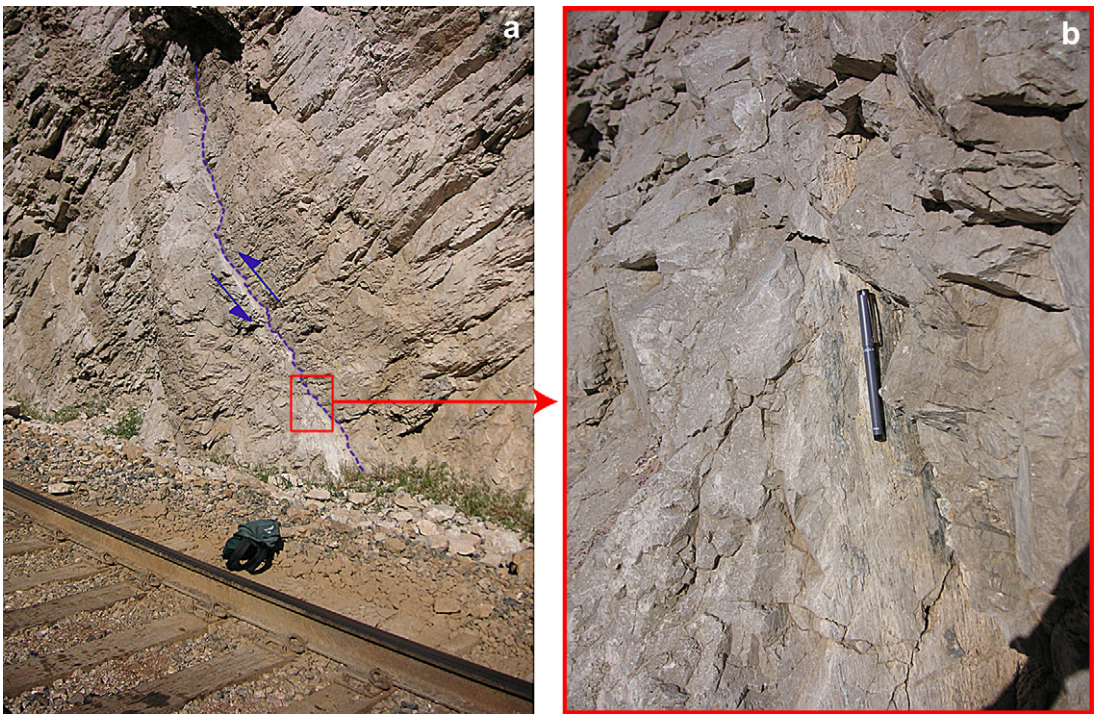

Fig. 16. (a) Bedding surface on the forelimb in the Madison Limestone exposed in the NW face of the Bighorn River canyon (see Fig. 1). Blue dashed line highlights bedding surface; blue arrows show the sense of motion. (b) Closer view of the slickenlines on bedding surface outlined by the red box in (a). The relative motion was directed along the dip.

Here we compare bedding slip evolution for purely elastic and elastoplastic constitutive models for the outer layers (Fig. 13). Initially, when the outer layers respond elastically, bedding slip for the elastic and elastoplastic solutions are the same. As the fold grows in association with greater shortening (e.g., $\varepsilon = 1.5\%$ vs. $\varepsilon = 3.0\%$) and plastic deformation develops in the outer layers, the tangent stiffness deteriorates and the bedding-slip difference between the two cases increases (Fig. 13). At this stage of the deformation process (i.e., $\varepsilon = 3.0\%$) the reduction in the elastoplastic stiffness is such that the result compares well with the elastic solution that has a 50% lesser initial stiffness (Fig. 13). In the case of bulk plasticity, r represents the ratio between the elastic stiffness of the middle layer and the initial elastic stiffness of the outer layers (a parameter of the elastoplastic constitutive model).

The elastic analysis shows that as the stiffness of the outer layers decreases (r increases) the opening of hinge fractures becomes greater (Fig. 14a). A similar effect is observed when an elastoplastic rheology is prescribed for the outer layers (Fig. 14b). As the outer elastoplastic layers experience degradation of the tangent stiffness upon yielding the hinge fractures open significantly more than for the purely elastic counterpart. For instance when $r = 2$ and $\varepsilon = 3.0\%$ the stiffness reduction is such that hinge fractures open appreciably more than the opening produced by an elastic solution with a stiffness that is 20% of the initial stiffness ($r = 10$). Fracture opening for both plastic models ($r = 2$ and $r = 10$) are very similar when $\varepsilon = 3.0\%$ (Fig. 14b). This indicates that in the hinge area the outer layers of both models are deforming plastically with little change in stresses resolved onto the middle layer.

6. Comparison of field data and model results

The configuration and dimensions of the two-dimensional finite element models are comparable with a portion of the stratigraphic section in cross sections of SMA (Forster et al., 1996; Bellahsen et al., 2006). To a first order, model results reproduce field observations of Set I fractures, indicating that the modeling captures the basic evolution of these fractures as they were rotated and reactivated during folding. It should be understood that Set I fractures strike 110° when unfolded whereas the fold axis trends 135°. The two-dimensional model represents fractures as though they strike parallel to the fold axis, so it does not represent precisely the mechanical behavior of Set I fractures as influenced by this obliquity. Nevertheless, the results suggest that the development of a fold like SMA should induce dip-slip shearing along fractures in the forelimb and (to a lesser extent) backlimb, while producing fracture opening in the hinge. Field observations of fracture surfaces and thin section analyses indicate that dip-slip shearing has occurred along Set I fractures in the forelimb at SMA within all studied Formations: Madison, Tensleep (Fig. 15), and Phosphoria (Bellahsen et al., 2006). No conclusive evidence for dip-slip shearing along Set I fractures has been found in the backlimb or the hinge. Fig. 10 indicates that for a given applied contraction, less offset occurs along fractures in the backlimb than in the forelimb. This offset in the backlimb may have been unnoticeable in the field, or alternatively, the dip-slip offset may be insignificant relative to, and thus masked by, the prominent strike-slip offset on Set I fractures (Fiore, 2006).

Set I fractures in the hinge do not have apertures noticeably larger than those in the backlimb or forelimb, but neither are they parallel to the fold axis. Set III fractures that do strike parallel to the trend of the anticline are found only in the hinge and have been interpreted to have formed in response to bending stresses during folding (Bellahsen et al., 2006). The formation and opening of Set III fractures in the hinge are consistent with the model results.

In the forelimb, slickenlines along bedding surfaces in the Madison Fm. (Fig. 16), tail cracks emanating from bedding surfaces in the Phosphoria Fm. (Fig. 17a,b), and polished bedding surfaces of the Phosphoria Fm. (Fig. 17c) all indicate that bed-parallel slip has accompanied the folding at SMA. No indicators of bed-parallel slip were observed in either the hinge or the backlimb. These field observations are in agreement with the model result that greater bed-parallel slip occurs in the forelimb than in the hinge or backlimb.

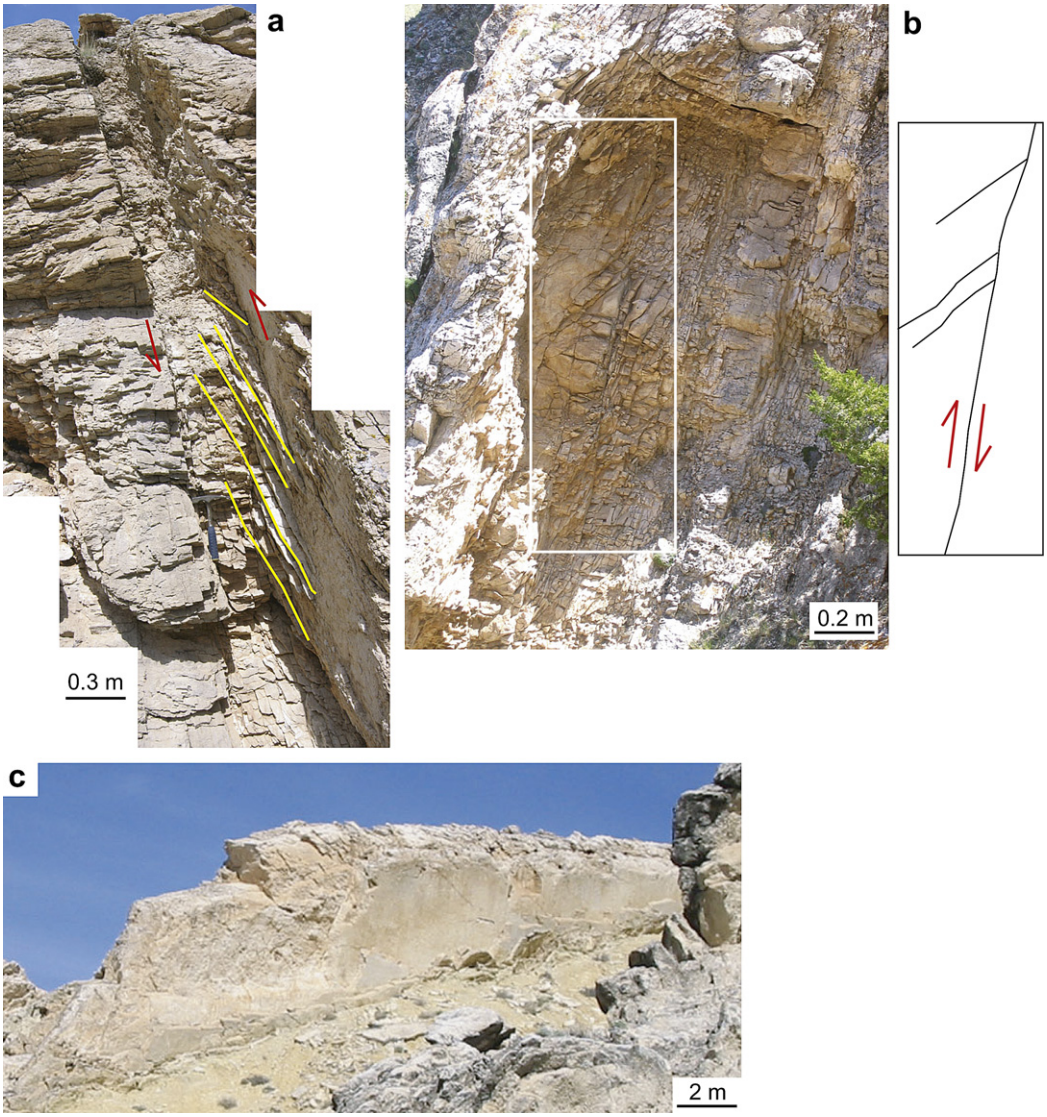

Fig. 17. (a) Splay cracks between bedding surfaces in the forelimb provide evidence for bedding plane slip in the Phosphoria Formation. Yellow lines highlight splay cracks; red arrows show the interpreted direction of motion. (b) Splay cracks between bedding surfaces in the forelimb (Phosphoria Formation). Inset interpretation shows the orientation of a bedding plane and related splays and the direction of shearing. (c) Polished undersides of bedding planes in the forelimb (Phosphoria Formation) provide evidence for bed-parallel slip as one mechanism of folding at SMA.

7. Conclusions

Non-linear finite element modeling combined with large deformation frictional contact mechanics is a powerful tool for the analysis of complex geological processes such as the reactivation of fractures in both sliding and opening, and the evolution of bed-parallel slip during folding of an asymmetric anticline. A variety of numerical models were developed to illustrate the effects of mechanical stratigraphy, slip on bedding surfaces, and net contraction during folding on the response of the system. The results of the FEM model correspond with selected field observations and provide additional insights about the physics of the folding process. The results indicate that fractures located in the hinge and striking parallel to the fold axis should open; that fractures in the limbs are primarily reactivated by shearing as thrust faults; and that slip on fractures and along bedding surfaces should be more significant in the steeper dipping forelimb than in the shallower dipping backlimb. These numerical results are in qualitative agreement with field observations of Set I and Set III fractures at Sheep Mountain Anticline. We also demonstrate that when the stratigraphic units surrounding a fractured unit are softer, the flexural-slip mechanism is less significant, because it is easier to deform the softer layers than to overcome friction and induce slip along the bedding surfaces. In contrast, when there is not a significant distinction in the mechanical properties of rock layers ($0.5 < r < 2$), bed-parallel slip becomes important and it greatly affects the response of the fractures.

The findings given here leave obvious room for extension, both in analysis and in modeling. For instance, this work does not address three-dimensional effects and the nucleation and propagation of new fracture sets during folding which could alter the reactivation of preexisting fractures. A different, but equally interesting extension would consist in relaxing the rate-independent hypothesis (elasticity and plasticity) for rock behavior, resulting in more advanced constitutive formulations capable of capturing strain-rate-dependent deformation. However, these potential extensions would result in more complex models, making the analysis even more difficult, and hence, making it much more challenging to identify those factors which play the leading role in governing the mechanics of folding and fracturing. The work presented here should be seen as an attempt to reproduce, in a simple

yet meaningful manner, the mechanics of a complex geologic phenomenon.

Acknowledgments

Support for this research was provided by National Science Foundation Grant No. CMG-0417521 (Collaborations in Mathematical Geosciences) and US Department of Energy Grant No.DE-FG02-03ER15454. The authors wish to thank graduate student Peter Lovely for the meticulous review of the manuscript. We also thank William Dunne, Mark Fischer, and Peter Hudleston for their insightful reviews and comments.

References

Anderson, T.L., 1995. Fracture Mechanics: Fundamentals and Applications. CRC Press, Boca Raton, 688 pp.
Aydin, A., 2000. Fractures, faults, and hydrocarbon entrapment, migration and flow. Marine and Petroleum Geology 17, 797–814.
Bai, T., Pollard, D.D., 2000. Fracture spacing in layered rocks: a new explanation based on the stress transition. Journal of Structural Geology 22, 43–57.
Bai, T., Pollard, D.D., Gao, H., 2000. Explanation for fracture spacing in layered materials. Nature 403, 753–756.
Behzadi, H., Dubey, A.K., 1980. Variation of interlayer slip in space and time during flexural folding. Journal of Structural Geology 2, 453–457.
Bellahsen, N., Fiore, P., Pollard, D.D., 2006. The role of fractures in the structural interpretation of Sheep Mountain Anticline, Wyoming. Journal of Structural Geology 28, 850–867.
Bieniawski, Z.T., 1978. Determining rock mass deformability: experience from case histories. International Journal of Rock Mechanics and Mining Sciences and Geomechanics Abstracts 15, 237–248.
Bird, P., 2002. Stress direction history of the Western United States and Mexico since 85 Ma. Tectonics 21, 1014, doi:10.1019/2001TC001319.
Bobillo-Ares, N.C., Bastida, F., Aller, J., 2000. On tangential longitudinal strain folding. Tectonophysics 319, 53–68.
Borja, R.I., 2006. Conditions for instabilities in collapsible solids including volume implosion and compaction banding. Acta Geotechnica 1, 107–122.
Borja, R.I., Sama, K.M., Sanz, P.F., 2003. On the numerical integration of three-invariant elastoplastic constitutive models. Computer Methods in Applied Mechanics and Engineering 192, 1227–1258.
Bourne, S.J., 2003. Contrast of elastic properties between rock layers as a mechanism for the initiation and orientation of tensile failure under remote compression. Journal of Geophysical Research 108, 2395.
Byerlee, J.D., 1978. Friction of rocks. Pure and Applied Geophysics 116, 615–626.
Carmichael, R.S., 1982. Handbook of Physical Properties of Rocks. CRC Press, Boca Raton, FL.
Casey, M., Butler, R.W.H., 2004. Modelling approaches to understanding fold development: implications for hydrocarbon reservoirs. Marine and Petroleum Geology 21, 933–946.
Cooke, M.L., Pollard, D.D., 1997. Bedding-plane slip in initial stages of fault-related folding. Journal of Structural Geology 19, 567–581.
Cooke, M.L., Underwood, C.A., 2001. Fracture termination and step-over at bedding interfaces due to frictional slip and interface opening. Journal of Structural Geology 23, 223–238.
Cooke, M.L., Mollema, P., Pollard, D.D., Aydin, A., 2000. Interlayer slip and joint localization in East Kaibab Monocline, Utah: field evidence and results from numerical modeling. In: Cosgrove, J.W., Ameen, M.S. (Eds.), Forced Folds and Fractures. Geological Society Special Publication 169, London, pp. 23–49.
Couples, G.D., Lewis, H., 2000. Effects of interlayer slip in model forced folds. In: Cosgrove, J.W., Ameen, M.S. (Eds.), Forced Folds and Fractures. Geological Society Special Publication 169, London, pp. 129–144.
Coward, M.P., Daltaban, T.S., Johnson, H., 1998. Structural Geology in Reservoir Characterization. Geological Society Special Publication 127, London, 266 pp.
Crook, A.J.L., Owen, D.R.J., Willson, S.M., Yu, J.G., 2006a. Benchmarks for the evolution of shear localisation with large relative sliding in frictional materials. Computer Methods in Applied Mechanics and Engineering 195, 4991–5010.
Crook, A.J.L., Willson, S.M., Yu, J.G., Owen, D.R.J., 2006b. Predictive modelling of structure evolution in sandbox experiments. Journal of Structural Geology 28, 729–744.
Cruikshank, K.M., Aydin, A., 1995. Unweaving the joints in Entrada Sandstone, Arches National Park, Utah, USA. Journal of Structural Geology 17, 409–421.
Cruikshank, K.M., Zhao, G., Johnson, A.M., 1991. Analysis of minor fractures associated with joints and faulted joints. Journal of Structural Geology 13, 865–886.
Engebretson, D.C., Cox, A., Gordon, R.G., 1985. Relative motion between oceanic and continental plates in the Pacific basin. Geological Society of America Special Paper 206, 59.
Engelder, T., Peacock, D.C.P., 2001. Joint development normal to regional compression during flexural-flow folding: the Lilstock buttress anticline, Somerset, England. Journal of Structural Geology 23, 259–277.
Erickson, S.G., Jamison, W.R., 1995. Viscous-plastic finite-element models of fault-bend folds. Journal of Structural Geology 17, 561–573.
Erickson, S.G., Strayer, L.M., Suppe, J., 2001. Initiation and reactivation of faults during movement over thrust-fault ramp: numerical mechanical models. Journal of Structural Geology 23, 11–23.
Fiore, P.E., 2006. 3D characterization and mechanics of brittle deformation in thrust fault related folds. PhD thesis, Stanford University, California, USA.
Fischer, M.P., Wilkerson, M.S., 2000. Predicting the orientation of joints from fold shape: results of pseudo-three-dimensional modeling and curvature analysis. Geology 28, 15–18.
Fischer, M.P., Woodward, N.B., 1992. The geometric evolution of foreland thrust systems. In: McClay, K.R. (Ed.), Thrust Tectonics. Chapman and Hall, London, pp. 181–189.
Fisher, D.M., Anastasio, D.J., 1994. Kinematic analysis of a large-scale leading edge fold, Lost River Range, Idaho. Journal of Structural Geology 16, 337–354.
Forster, A., Irmen, A.P., Vondra, C., 1996. Structural interpretation of Sheep Mountain Anticline, Bighorn Basin, Wyoming. Wyoming Geological Association Guidebook 47, 239–251.
Goodman, R.E., 1989. Introduction to Rock Mechanics, second ed. John Wiley & Sons, pp. 141-150195-250.
Griffith, A.A., 1921. The phenomena of rupture and flow in solids. Royal Society of London Transactions 221, 163–178.
Guiton, M., Leroy, Y., Sassi, W., 2003a. Activation of diffuse discontinuities and folding of the sedimentary layers. Journal of Geophysical Research 108, 2183, doi:10.1029/2002JB001770.
Guiton, M., Sassi, W., Leroy, Y., Gauthier, B., 2003b. Mechanical constraints on the chronology of fracture activation in the folded Devonian sandstone of the western Moroccan Anti-Atlas. Journal of Structural Geology 25, 1317–1330.
Haneberg, W.C., Mosley, P.S., Moore, J.C., Goodwin, L.B., 1999. Faults and subsurface fluid flow in the shallow crust. In: Geophysical Monograph Series. American Geophysical Union, Washington, DC, 222 pp.
Hennier, J., Spang, J., 1983. Mechanisms for deformation of sedimentary strata at Sheep Mountain anticline, Big Horn Basin, Wyoming. Wyoming Geological Association Guidebook, 34th Annual Field Conference, pp. 97–111.
Horne, R., Culshaw, N., 2001. Flexural-slip folding in the Meguma Group, Nova Scotia, Canada. Journal of Structural Geology 23, 1631–1652.
Jaeger, J.C., Cook, N.G.W., 1969. Fundamentals of Rock Mechanics. Chapman and Hall, New York, pp. 53-76.
Johnson, A.M., 1977. Styles of Folding. Elsevier, New York, 406 pp.
Johnson, A.M., Fletcher, R.C., 1994. Folding of Viscous Layers. Columbia University, New York, 461 pp.
Johnson, K.M., Johnson, A.M., 2000. Localization of layer-parallel faults in San Rafael swell, Utah and other monoclinal folds. Journal of Structural Geology 22, 1455–1468.
Jones, G., Fisher, Q.J., Knipe, R.J., 1998. Faulting, Fault Sealing and Fluid Flow in Hydrocarbon Reservoirs. Geological Society Special Publication 147, London, 319 pp.
Kuenen, P.H., de Sitter, L.U., 1938. Experimental investigation into the mechanisms of folding. Leidshe Geologische Mededeelingen 10, 217–240.
Ladd, R.E., 1979. The geology of Sheep Canyon Quadrangle: Wyoming. Iowa State University, PhD dissertation. Ames. 124pp.
Laursen, T.A., 2002. Computational Contact and Impact Mechanics. Springer, Berlin and Heidelberg.
Laursen, T.A., Simo, J.C., 1993. A continuum-based finite element formulation for the implicit solution of multibody large deformation frictional contact problems. International Journal for Numerical Methods in Engineering 36, 3451–3485.
Lawn, B.R., Wilshaw, T.R., 1975. Fracture of Brittle Solids. Cambridge University Press, Cambridge, 204 pp.
Matsuoka, H., Nakai, T., 1974. Stress-deformation and strength characteristics of soils under three different principal stresses. Proceedings of Japan Society of Civil Engineers 232, 59–70.
Maerten, L., Maerten, F., 2006. Chronologic modeling of faulted and fractured reservoirs using geomechanically based restoration: Technique and industry applications. AAPG Bulletin 90, 1201–1226.
McConaughy, D.T., Engelder, T., 2001. Joint initiation in bedded clastic rocks. Journal of Structural Geology 23, 203–221.
Mühlhaus, H.-B., Dufour, F., Moresi, L., Hobbs, B., 2002. A director theory for visco-elastic folding instabilities in multilayered rock. International Journal of Solids and Structures 39, 3675–3691.
Müller, J., 1979. Contributions to engineering geology and slope movement investigations. In: Voight, B. (Ed.), Rockslides and Avalanches, part 2. Elsevier, New York, pp. 95–109.
National Research Council, 1996. Rock Fractures and Fluid Flow—Contemporary Understanding and Applications. National Academy Press, Washington, DC, 551 pp.
Nino, F., Philip, H., Chery, J., 1998. The role of bed-parallel slip in the formation of blind thrust faults. Journal of Structural Geology 20, 503–516.
Pfaff, V.J., Johnson, A.M., 1989. Opposite senses of fold asymmetry. Engineering Geology 27, 3–38.
Pollard, D.D., Aydin, A., 1988. Progress in understanding jointing over the past century. Geological Society of America Bulletin 100, 1181–1204.
Pollard, D.D., Fletcher, R.C., 2005. Fundamentals of Structural Geology. Cambridge University Press, pp. 321-322.

Ramsay, J.G., 1974. Development of chevron folds. Geological Society of America Bulletin 85, 1741–1754.
Renshaw, C.E., Pollard, D.D., 1994. Numerical simulation of fracture set formation: A fracture mechanics model consistent with experimental observations. Journal of Geophysical Research 99 (B5), 9359–9372.
Rioux, R.L., 1958. Geology of the Spence-Kane area, Bighorn County, Wyoming. Unpublished Ph.D. thesis, University of Illinois, 182 pp.
Rioux, R.L., 1994. Geologic map of the Sheep Mountain-Little Sheep Mountain area, Big Horn County, Wyoming. Scale 1 (31), 680. USGS open-file report 94–191.
Sanz, P.F., Borja, R.I., Pollard, D.D., 2007. Mechanical aspects of thrust faulting driven by far-field compression and their implications to fold geometry. Acta Geotechnica 2, 17–31.
Simo, J.C., Taylor, R.L., 1985. Consistent tangent operators for rate-independent elastoplasticity. Computer Methods in Applied Mechanics and Engineering 48, 101–118.
Smith, D.A., 1966. Theoretical considerations of sealing and non-sealing faults. AAPG Bulletin 50, 363–374.
Suppe, J., 1985. Principles of Structural Geology. Prentice-Hall, Englewood Cliffs, NJ, 537 pp.
Stanton, H.I., Erslev, E.A., 2004. Sheep Mountain Anticline: backlimb tightening and sequential deformation in the Bighorn Basin, Wyoming. Wyoming Geological Association Guidebook 53, 75–87.
Strayer, L.M., Hudleston, P.J., 1997. Numerical modeling of fold initiations at thrust ramps. Journal of Structural Geology 19, 551–566.
Treagus, S.H., 1988. Strain refraction in layered systems. Journal of Structural Geology 10, 517–527.
Wickham, J.S., Tapp, G.S., Reddy, J.N., 1982. Finite-element modelling of fracture density in single layer folds. International Journal for Numerical and Analytical Methods in Geomechanics 6, 441–459.
Wilkins, S.J.G., Michael, R., Wacker, M., Eyal, Y., Engelder, T., 2001. Faulted joints; kinematics, displacement-length scaling relations and criteria for their identification. Journal of Structural Geology 23, 315–327.
Wriggers, P., 1995. Finite element algorithms for contact problems. Archives of Computational Methods in Engineering 4, 1–49.
Wriggers, P., 2002. Computational Contact Mechanics. Wiley, Chichester.